DISCOVERY OF MAIN-BELT COMET P/2006 VW139 BY Pan-STARRS1

Henry H. Hsieh[1,16], Bin Yang[1], Nader Haghighipour[1], Heather M. Kaluna[1], Alan Fitzsimmons[2], Larry Denneau[1], Bojan Novaković[3], Robert Jedicke[1], Richard J. Wainscoat[1], James D. Armstrong[1,4], Samuel R. Duddy[5], Stephen C. Lowry[5], Chadwick A. Trujillo[6], Marco Micheli[1], Jacqueline V. Keane[1], Laurie Urban[1], Timm Riesen[1], Karen J. Meech[1], Shinsuke Abe[7], Yu-Chi Cheng[7], Wen-Ping Chen[7], Mikael Granvik[8], Tommy Grav[9], Wing-Huen Ip[7], Daisuke Kinoshita[7], Jan Kleyna[1], Pedro Lacerda[2,17], Tim Lister[4], Andrea Milani[10], David J. Tholen[1], Peter Vereš[1], Carey M. Lisse[11], Michael S. Kelley[12], Yanga R. Fernández[13], Bhuwan C. Bhatt[14], Devendra K. Sahu[14], Nick Kaiser[1], K. C. Chambers[1], Klaus W. Hodapp[1], Eugene A. Magnier[1], Paul A. Price[15], and John L. Tonry[1]

[1] Institute for Astronomy, University of Hawaii, 2680 Woodlawn Drive, Honolulu, HI 96822, USA; hsieh@ifa.hawaii.edu
[2] Astrophysics Research Centre, Queens University Belfast, Belfast BT7 1NN, UK
[3] Department of Astronomy, Faculty of Mathematics, University of Belgrade, Studentski trg 16, 11000 Belgrade, Serbia
[4] Las Cumbres Observatory Global Telescope Network, Inc., 6740 Cortona Dr. Suite 102, Santa Barbara, CA 93117, USA
[5] Centre for Astrophysics and Planetary Science, The University of Kent, Canterbury CT2 7NH, UK
[6] Gemini Observatory, Northern Operations Center, 670 N. Aohoku Place, Hilo, HI 96720, USA
[7] Institute of Astronomy, National Central University, 300 Jhongda Rd, Jhongli 32001, Taiwan
[8] Department of Physics, 00014 University of Helsinki, P.O. Box 64, Helsinki, Finland
[9] Planetary Science Institute, 1700 East Fort Lowell, Suite 106, Tucson, AZ 85719, USA
[10] Dipartimento di Matematica, Università di Pisa, Largo Pontecorvo 5, 56127 Pisa, Italy
[11] Planetary Exploration Group, Space Department, Johns Hopkins University Applied Physics Laboratory, Laurel, MD 20723, USA
[12] Department of Astronomy, University of Maryland, College Park, MD 20742, USA
[13] Department of Physics, University of Central Florida, 4000 Central Florida Blvd., Orlando, FL 32816, USA
[14] Indian Institute of Astrophysics, CREST Campus, Block-II, Koramangala, Sarjapur Road, Bangalore 560034, India
[15] Department of Astrophysical Sciences, Peyton Hall, Princeton University, Princeton, NJ 08544, USA

ABSTRACT

The main-belt asteroid (300163) 2006 VW139 (later designated P/2006 VW139) was discovered to exhibit comet-like activity by the Pan-STARRS1 (PS1) survey telescope using automated point-spread-function analyses performed by PS1's Moving Object Processing System. Deep follow-up observations show both a short ($\sim10''$) antisolar dust tail and a longer ($\sim60''$) dust trail aligned with the object's orbit plane, similar to the morphology observed for another main-belt comet (MBC), P/2010 R2 (La Sagra), and other well-established comets, implying the action of a long-lived, sublimation-driven emission event. Photometry showing the brightness of the near-nucleus coma remaining constant over ~30 days provides further evidence for this object's cometary nature, suggesting it is in fact an MBC, and not a disrupted asteroid. A spectroscopic search for CN emission was unsuccessful, though we find an upper limit CN production rate of $Q_{CN} < 1.3 \times 10^{24}$ mol s^{-1}, from which we infer a water production rate of $Q_{H_2O} < 10^{26}$ mol s^{-1}. We also find an approximately linear optical spectral slope of 7.2%/1000 Å, similar to other cometary dust comae. Numerical simulations indicate that P/2006 VW139 is dynamically stable for >100 Myr, while a search for a potential asteroid family around the object reveals a cluster of 24 asteroids within a cutoff distance of 68 m s^{-1}. At 70 m s^{-1}, this cluster merges with the Themis family, suggesting that it could be similar to the Beagle family to which another MBC, 133P/Elst-Pizarro, belongs.

Key words: comets: general – minor planets, asteroids: general

Online-only material: color figures

1. INTRODUCTION

Main-belt comets (MBCs) exhibit cometary activity indicative of ice sublimation yet are dynamically indistinguishable from main-belt asteroids (Hsieh & Jewitt 2006). Much of the current interest in studying MBCs lies in the possible role of main-belt objects in the primordial delivery of terrestrial water (e.g., Morbidelli et al. 2000). Of the first five known MBCs, one (176P/LINEAR) was discovered via a targeted search (Hsieh 2009), while the other four were discovered serendipitously or by untargeted surveys (Elst et al. 1996; Read et al. 2005; Garradd et al. 2008; Nomen et al. 2010). Using MBCs as tracers of ice in the asteroid belt to ascertain its potential for water delivery will require a much larger sample of these objects, and as such, discovering more MBCs, ideally in untargeted surveys

(e.g., Gilbert & Wiegert 2009; Sonnett et al. 2011), is a high priority.

Recently, main-belt objects P/2010 A2 (LINEAR) and (596) Scheila have exhibited comet-like dust emission, but these events are likely due to impact-generated ejecta clouds (Jewitt et al. 2010, 2011; Snodgrass et al. 2010; Bodewits et al. 2011; Yang & Hsieh 2011; Ishiguro et al. 2011; Hainaut et al. 2012). As such, these objects are better characterized as disrupted asteroids. Hsieh et al. (2012a) considered the problem of distinguishing MBCs and disrupted asteroids, and concluded that recurrent activity separated by periods of inactivity to be the strongest observable indicator that activity is sublimation-driven, particularly when the timing of active episodes corresponds closely to an object's orbital period (cf. 133P/Elst-Pizarro and 238P/Read; Hsieh et al. 2004, 2010, 2011c). Evaluating this criterion requires monitoring an object for many years, however. When observations of only one active episode for an object are available, Hsieh et al. (2012a) suggested that steady or

---

[16] Hubble Fellow.
[17] Michael West Fellow.

increasing activity and morphological indicators could be used as preliminary evidence of sublimation. Direct spectroscopic detection of sublimation products (i.e., gas) in an MBC would immediately confirm its cometary nature. Given the difficulty of obtaining sufficiently high-quality spectroscopy of such distant and weakly active comets and of timing observations to coincide with peak gas production though, the absence of gas detections to date (Jewitt et al. 2009; Hsieh et al. 2012b) should not be considered confirmation of the absence of sublimation.

2. OBSERVATIONS

Observations of activity in P/2006 VW$_{139}$ were first obtained by the 1.8 m Pan-STARRS1 (PS1) wide-field synoptic survey telescope on Haleakala. PS1 employs a $3°2 \times 3°2$ 1.4 gigapixel camera, consisting of a mosaic of 60 orthogonal transfer arrays, each comprising 64 590×598 pixel CCDs, and Sloan Digital Sky Survey (SDSS) i'- and z'-band-like filters designated i_{P1} and z_{P1} (Tonry et al. 2012).

Follow-up imaging was performed using the 2.0 m Faulkes Telescope North (FTN) on Haleakala and Faulkes Telescope South (FTS) at Siding Spring, the University of Hawaii (UH) 2.2 m telescope on Mauna Kea, the 1.8 m Perkins Telescope (PT) at Lowell Observatory, the 2.0 m Himalayan Chandra Telescope (HCT) at the Indian Astronomical Observatory on Mt. Saraswati, the 4.2 m William Herschel Telescope (WHT; Program SW2011b20) at La Palma, the 3.54 m New Technology Telescope (NTT; Program 185.C-1033(K)) operated by the European Southern Observatory (ESO) at La Silla, and the Lulin One-meter Telescope (LOT) in Taiwan. We employed 4096×4096 pixel Fairchild CCDs and either SDSS or Bessell filters for Faulkes observations, a 2048×2048 pixel Textronix CCD and Kron-Cousins filters for UH observations, the Perkins ReImaging System and Kron–Cousins filters for Perkins observations, a 2048×2048 pixel E2V CCD and Bessell filters for HCT observations, the WHT's auxiliary-port camera (ACAM; Benn et al. 2008) and SDSS filters on the WHT, the ESO Faint Object Spectrograph and Camera (Buzzoni et al. 1984) and Bessell filters on the NTT, and a VersArray:1300B CCD (Kinoshita et al. 2005) and Bessell-like filters on the LOT.

We performed standard bias subtraction and flat-field reduction (using dithered twilight sky images) for all data, except those from PS1, using Image Reduction and Analysis Facility (IRAF) software. PS1 data were reduced using the system's image processing pipeline (IPP; Magnier 2006). Photometry of Landolt (1992) standard stars and field stars was performed by measuring net fluxes within circular apertures, with background sampled from surrounding circular annuli. For data obtained under non-photometric conditions, absolute calibration was accomplished using SDSS field star magnitudes (Aihara et al. 2011). Conversion of r'-band PS1, FTN, FTS, and WHT photometry to R-band was accomplished using transformations derived by Tonry et al. (2012) and by R. Lupton (http://www.sdss.org/). Comet photometry was performed using circular apertures with varying radii depending on the nightly seeing, where background statistics were measured in nearby, but non-adjacent, regions of blank sky to avoid dust contamination from the comet.

We also obtained long-slit spectroscopy with ACAM (3500–9400 Å) on the WHT, as well as with the Gemini Multi-Object Spectrographs (GMOS; 3600–9400 Å; Hook et al. 2004) on the 8 m Gemini North (GN; Program GN-2011B-Q-16) and Gemini South (GS; Program GS-2011B-Q-51) observatories. For ACAM observations, we employed a $2''0$ wide slit, giving a spectral resolution of $R \sim 300$, aligned with the object's dust tail. For GMOS observations, we employed B600 dispersers, 2×2 binning, and $1''0$ wide slits, giving $R \sim 850$, aligned with the dust trail. Reduction of GMOS data was performed using an IRAF package provided by Gemini.

3. RESULTS

3.1. Discovery of Cometary Activity

All PS1 moving object detections are screened for potential cometary activity by automated point-spread function (PSF) analyses executed nightly by PS1's Moving Object Processing System (MOPS). This screening process divides the measured second PSF moment of each transient source by the expected PSF width as determined from the median of all stellar PSFs in the field. This "psfextent" parameter is then plotted as a function of a detection quality parameter ("psfquality") ranging from 0 to 1, roughly corresponding to a normalized signal-to-noise ratio. Sources that show comet-like psfextent parameters and psfquality > 0.5 (to screen out faint sources for which measured PSF moments are unreliable) are flagged for human inspection and possible observational follow-up (Figure 1).

PS1 observations on 2011 November 5 showed that the PSF of the known main-belt asteroid, (300163) 2006 VW$_{139}$ (semimajor axis, $a = 3.052$ AU; eccentricity, $e = 0.201$; and inclination, $i = 3°24$), had an FWHM of $1''3$, while nearby stars had PSFs with FWHMs of $1''0$ (Hsieh et al. 2011a). Precovery observations also obtained by PS1 showed that the object exhibited a similar PSF excess on 2011 August 30. At the time, however, the object was too faint (psfquality < 0.5) and was not flagged for inspection. In both the relatively shallow August and November PS1 data, no extended cometary features were seen. Deeper follow-up observations (Table 1), however, revealed the presence of both an antisolar dust tail and an orbit-aligned dust trail (Figure 2; Section 3.2), leading to the object's re-designation as P/2006 VW$_{139}$.

3.2. Morphological and Photometric Analysis

The morphology observed for P/2006 VW$_{139}$ from mid-November 2011 through 2012 January (shortly after perihelion) remains approximately constant (Figure 2). We observe the presence of a short dust tail ($\sim 10''$) pointed in the antisolar direction, a longer dust trail ($\sim 60''$) aligned with the object's orbit plane, and a coma with an intrinsic FWHM of $\sim 0''7$ when deconvolved with the seeing. This morphology is similar to that observed for MBC P/2010 R2 (La Sagra) (Hsieh et al. 2012b), as well as other well-established comets (e.g., 2P/Encke, C/Austin 1990 V; Lisse et al. 1998; Reach et al. 2000). Detailed dust modeling will be required to confirm the nature of the observed dust features, but a simple syndyne plot (Figure 2; cf. Finson & Probstein 1968) indicates that the antisolar tail is likely composed of small particles with short dissipation times (requiring recent emission to still be present), while the orbit-aligned trail is composed of large particles with slow dissipation times (likely requiring months to traverse the observed distance from the nucleus). The contemporaneous observation of both recent and old dust emission implies the action of a prolonged event, consistent with sublimation and inconsistent with an impulsive impact. We furthermore compute that particles with radii of $a_d = 0.1 \,\mu$m should move $10''$ from the nucleus in just 22 days, creating an observable gap between the antisolar tail and the nucleus. No such gap is observed between November
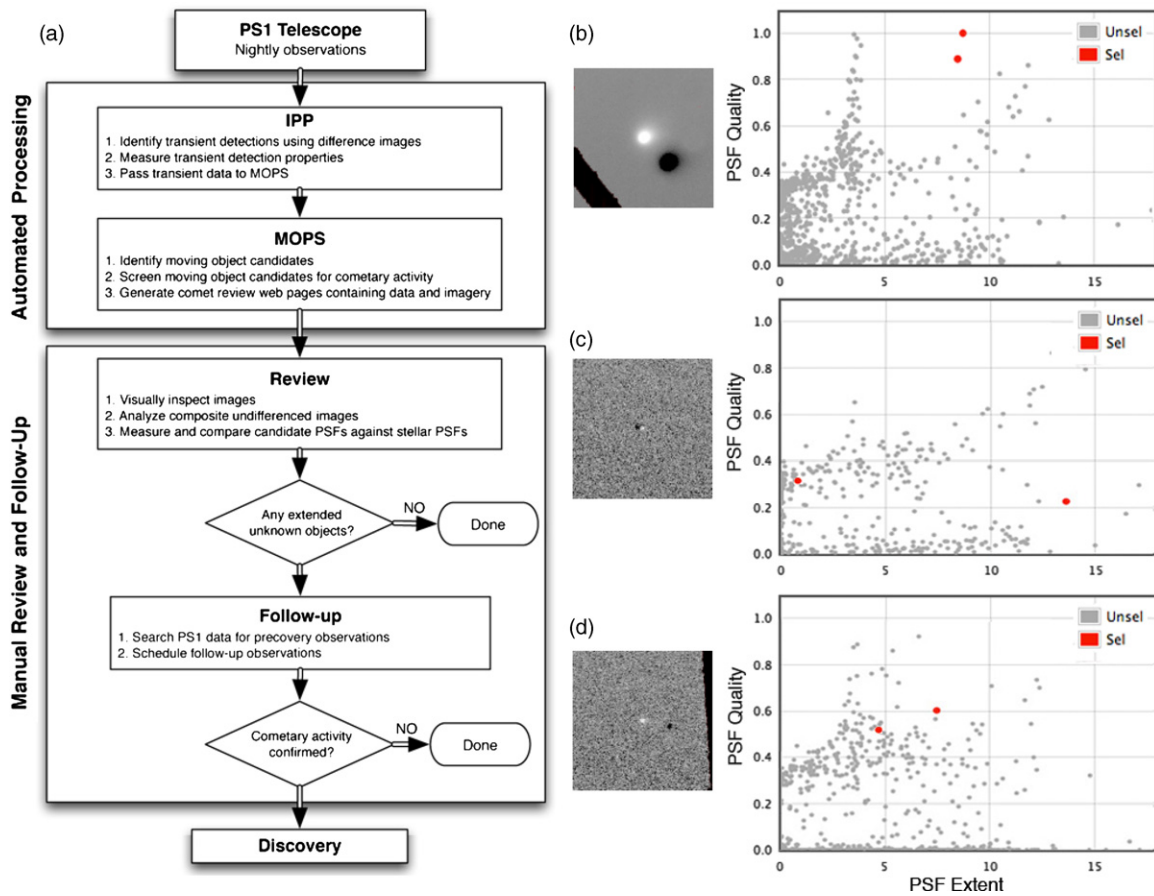
Figure 1. (a) Flowchart detailing PS1 comet screening procedures. (b) Difference image (left) and screening plot (right) for sample PS1 observations of 48P/Johnson where comet candidates ("selected") are plotted as red dots and "unselected" detections (generally consisting of inactive asteroids and false detections) are plotted as gray dots. (c) Image and screening plot for precovery observations of P/2006 VW_{139} on 2011 August 30. (d) Image and screening plot for discovery observations of P/2006 VW_{139} on 2011 November 5.

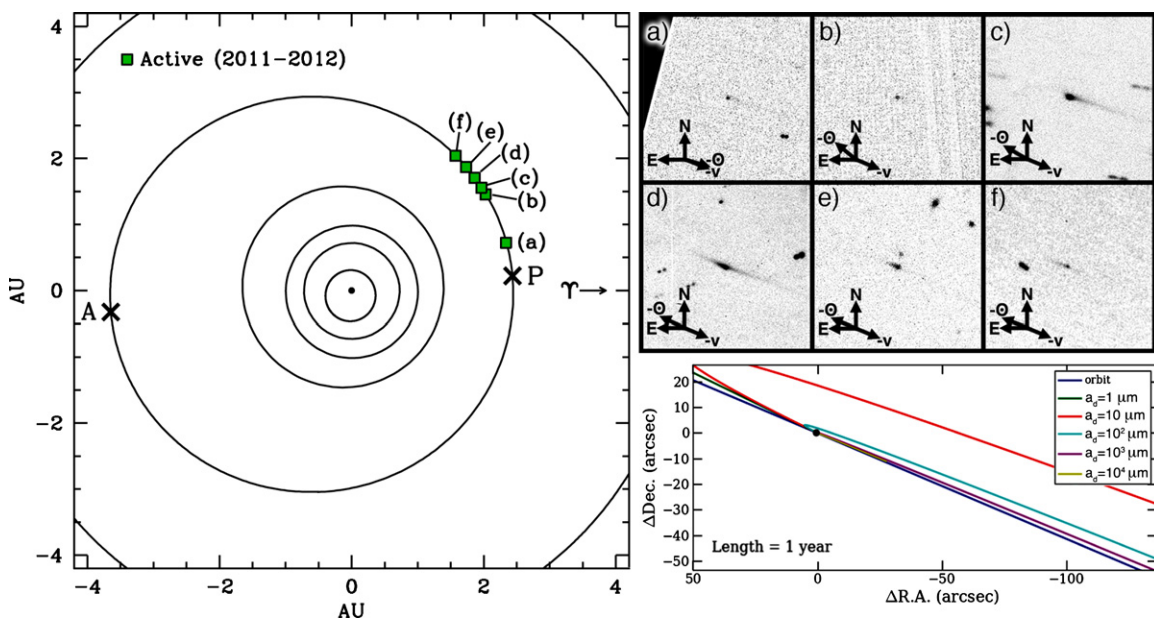(A color version of this figure is available in the online journal.)

Figure 2. Orbital position plot (left) and composite images (upper right) constructed from observations detailed in Table 1, with the Sun (black dot) at the center, and the orbits of Mercury, Venus, Earth, Mars, P/2006 VW_{139}, and Jupiter shown as black lines. Perihelion (P) and aphelion (A) are marked with crosses. Plotted positions and images correspond to observations from (a) 2011 August 30, (b) 2011 November 5, (c) 2011 November 12–14 (November 14 UH composite image shown), (d) 2011 November 22–December 4 (December 4 NTT composite image shown), (e) 2011 December 16–19 (December 19 UH composite image shown), and (f) 2012 January 7. Each panel is $90'' \times 90''$ with the object at the center, and north (N), east (E), the antisolar vector ($-\odot$), and the negative heliocentric velocity vector ($-v$) marked with arrows. Also shown is a syndyne plot (lower right) for the 2011 November 22–December 4 period for a range of dust grain radii.

(A color version of this figure is available in the online journal.)

Table 1
Observations

UT Date	Tel.[a]	N[b]	t[c]	Filter	R[d]	Δ[e]	α[f]	ν[g]	PA$_{-\odot}$[h]	PA$_{-v}$[i]	α_{pl}[j]	$m(R, \Delta, \alpha)$[k]	$m_R(1, 1, 0)$[l]
2011 Jul 18	*Perihelion.....................*				2.438	2.293	24.6	0.0	249.3	247.3	0.8	. . .	. . .
2011 Aug 30	PS1	2	60	z_{P1}	2.447	1.806	21.4	12.2	253.7	248.5	1.7	20.16 ± 0.14	15.6 ± 0.3
2011 Nov 05	PS1	2	90	i_{P1}	2.496	1.517	4.6	30.7	50.5	247.9	1.4	19.00 ± 0.09	15.1 ± 0.2
2011 Nov 12	FTN	11	660	r'	2.505	1.555	8.0	32.9	59.8	247.8	1.1	18.69 ± 0.09	15.1 ± 0.2
2011 Nov 14	UH	8	2400	R	2.506	1.561	8.4	33.2	60.4	247.7	1.1	18.62 ± 0.05	15.1 ± 0.2
2011 Nov 14	FTN	3	540	R	2.506	1.561	8.4	33.2	60.4	247.7	1.1	18.64 ± 0.05	15.1 ± 0.2
2011 Nov 18	PT	19	11100	R	2.510	1.586	10.0	34.3	62.2	247.7	0.9	18.60 ± 0.10	15.0 ± 0.2
2011 Nov 19	HCT	22	11400	R	2.512	1.596	10.6	34.6	62.8	247.6	0.9	18.64 ± 0.02	15.0 ± 0.2
2011 Nov 22	WHT	3	780	r'	2.516	1.621	11.9	35.5	63.8	247.6	0.8	18.89 ± 0.02	15.1 ± 0.2
2011 Nov 22	WHT	3	2700	spec.	2.516	1.621	11.9	35.5	63.8	247.6	0.8	. . .	. . .
2011 Nov 30	UH	5	3000	R	2.525	1.685	14.4	37.4	65.4	247.5	0.5	19.04 ± 0.02	15.1 ± 0.2
2011 Dec 02	GN	8	4800	spec.	2.527	1.704	15.0	38.0	65.7	247.5	0.4	. . .	. . .
2011 Dec 04	NTT	2	1200	R	2.530	1.724	15.6	38.5	66.0	247.4	0.4	19.12 ± 0.03	15.1 ± 0.2
2011 Dec 04	NTT	1	600	B	2.530	1.724	15.6	38.5	66.0	247.4	0.4	20.18 ± 0.03	. . .
2011 Dec 05	GS	6	3600	spec.	2.531	1.735	15.9	38.8	66.2	247.4	0.3	. . .	. . .
2011 Dec 16	FTS	12	720	r'	2.546	1.861	18.7	41.7	67.4	247.4	0.0	19.70 ± 0.09	15.3 ± 0.2
2011 Dec 19	UH	3	900	R	2.549	1.895	19.2	42.4	67.7	247.4	−0.1	19.68 ± 0.03	15.3 ± 0.2
2012 Jan 07	LOT	8	1440	R	2.577	2.152	21.7	47.4	69.2	247.6	−0.6	20.43 ± 0.10	15.7 ± 0.2
2014 Mar 13	*Aphelion........................*				3.660	2.697	4.5	180.0	278.6	294.1	−1.2	. . .	. . .
2016 Nov 08	*Perihelion.....................*				2.436	1.823	21.3	0.0	65.1	248.2	1.1	. . .	. . .

Notes.
[a] Telescope.
[b] Number of exposures.
[c] Total integration time, in seconds.
[d] Heliocentric distance, in AU.
[e] Geocentric distance, in AU.
[f] Solar phase angle (Sun–object–Earth), in degrees.
[g] True anomaly, in degrees.
[h] Position angle of the antisolar vector, in degrees east of north.
[i] Position angle of the negative velocity vector, in degrees east of north.
[j] Orbit plane angle, in degrees.
[k] Mean apparent magnitude in specified filter.
[l] Absolute R-band magnitude (at $R = \Delta = 1$ AU and $\alpha = 0°$), assuming solar colors and IAU H, G phase-darkening where $G = 0.15$, where the listed uncertainty is dominated by the estimated uncertainty in G.

and January, implying continuous replenishment of the tail over this period, again consistent with cometary activity.

The disrupted asteroid (596) Scheila exhibited a 30% decline in coma brightness in 8 days (Jewitt et al. 2011). Meanwhile, other established MBCs exhibited steady or increasing coma brightness over longer periods of time (cf. Hsieh et al. 2012b). Photometry of P/2006 VW$_{139}$ (Table 1) shows no decline in near-nucleus brightness over 29 days between November and early December (though does show a 40% decline over 34 days between December and January). Coupled with our morphological analysis, the coma's photometric behavior over this period provides further support for the observed activity's sublimation-driven nature.

For reference, we compute the dust-to-nucleus scattering surface area ratio, A_d/A_N, determined for other MBCs (cf. Hsieh et al. 2012b). Lacking independent constraints at this time, we use the absolute R-band magnitude, $H_R = 16.4$ mag, computed by Spahr et al. (2009) only using observations obtained well before activity was discovered, and find $A_d/A_N \sim 2.5$ during the object's peak observed activity in November. This level of dust production relative to nucleus size is comparable to that of 133P and 176P, but an order of magnitude lower than for other MBCs, 238P, P/2008 R1 (Garradd), and P/La Sagra (Hsieh et al. 2012b). Multi-filter NTT observations (Table 1) indicate that the near-nucleus coma has an approximately Solar color of $B - R = 1.06 \pm 0.04$, similar to other MBCs (Jewitt et al. 2009; Hsieh et al. 2009b, 2010, 2011b, 2012b)

3.3. Spectroscopic Analysis

WHT spectroscopy was extracted using an aperture 10″ long along the slit centered on the target. A spectrophotometric standard, Feige 15, and a G2V solar analog star, HD 28099, were observed to allow removal of atmospheric absorption features and calculation of the relative reflectance spectrum. The resulting spectrum (Figure 3(a)) is approximately linear with a red slope of 7.2%/1000 Å, similar to that seen in other cometary dust comae (Kolokolova et al. 2004).

Gemini spectroscopy was extracted using an aperture 5″.1 long along the slit. A G5V solar analog star, HD 10097, was observed for approximate flux calibration and to calculate the relative reflectance spectra. The resulting GN and GS spectra (Figure 3(b)) are very similar. Given its slightly higher signal-to-noise ratio, however, we use the GN spectrum to compute gas production rates.

We measure the standard errors in three wavelength regions 70 Å in width and adopt the largest σ of 0.057 as the observational uncertainty of the violet CN emission band. We then employ a simple Haser (1957) model to derive the CN production rate (cf. Hsieh et al. 2012a; Jewitt & Guilbert-Lepoutre 2012), using a resonance fluorescence efficiency of $g[1 \text{ AU}] = 3.63 \times 10^{-13}$ erg s^{-1} molecule^{-1} (Schleicher 2010). We find an upper limit to the CN production rate of $Q_{CN} < 1.3 \times 10^{24}$ mol s^{-1}. No physical constraints on the CN to water production rate ratio in MBCs are currently available, but adopting the
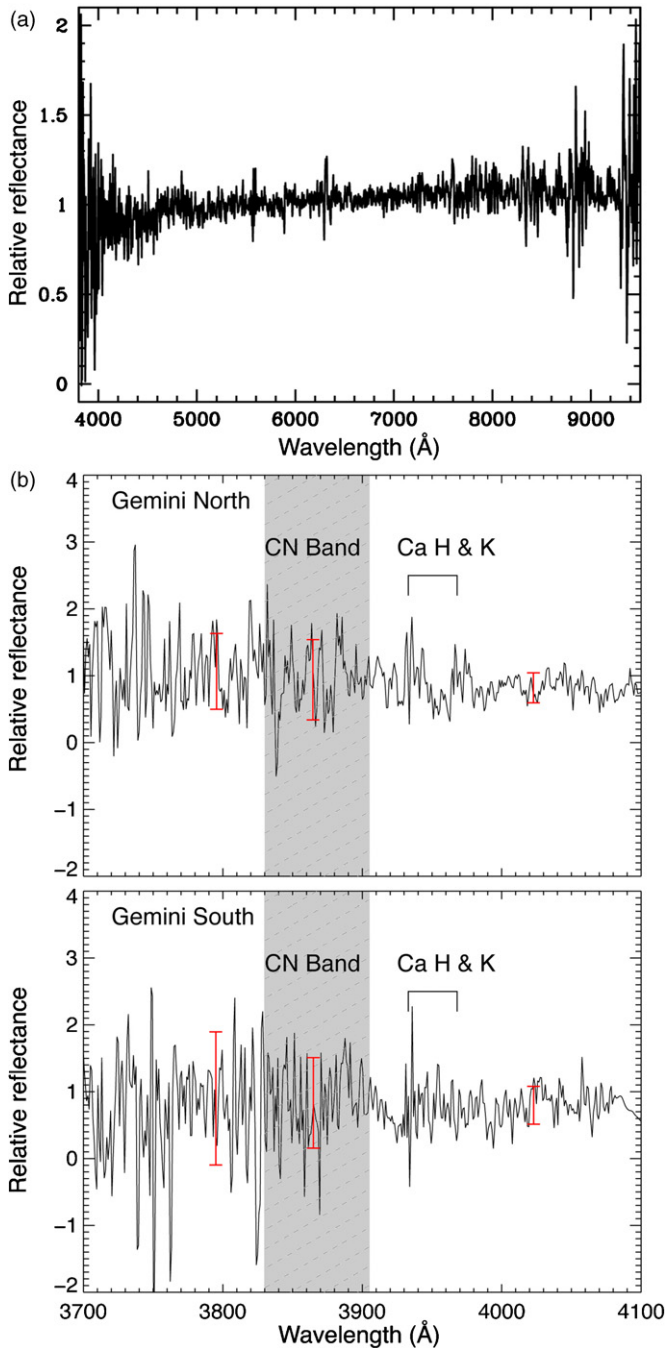
Figure 3. (a) Relative reflectance spectrum of P/2006 VW$_{139}$ from the WHT. (b) Relative reflectance spectra of P/2006 VW$_{139}$ from GN (upper panel) and GS (lower panel). Shaded regions indicate the wavelength region where the CN emission band is expected. Red error bars show 1σ uncertainties in the CN band region and in adjacent wavelength regions.

(A color version of this figure is available in the online journal.)

average ratio in other observed comets ($\log[Q_{CN}/Q_{OH}] = -2.5$; $Q_{OH}/Q_{H_2O} = 90\%$; cf. Hsieh et al. 2012a), we infer a water production rate of $Q_{H_2O} < 10^{26}$ mol s^{-1}.

3.4. Dynamical Analysis

To ascertain whether P/2006 VW$_{139}$ is likely to be native to its current location, we analyze its dynamical stability (cf. Jewitt et al. 2009; Hsieh et al. 2012a, 2012b). We produce nine randomly generated sets of 100 Gaussian-distributed massless

test particles in orbital element space, centered on the object's current osculating orbital elements, where three sets are characterized by σ values of $\sigma_a = 0.0001$ AU, $\sigma_e = 0.0001$, and $\sigma_i = 0°.001$. These σ values are chosen to adequately explore the stability of the region. As a numbered asteroid, P/2006 VW$_{139}$'s true orbital element uncertainties are actually $\sim100\times$–$1000\times$ smaller. Another three sets are characterized by σ values $10\times$ as large, and the final three sets are characterized by σ values $100\times$ as large. Treating the eight major planets as massive particles, we then use the N-body integration package, Mercury (Chambers 1999), to integrate the orbits of these test particles forward in time for 100 Myr. Limitations on computing resources unfortunately prevent us from conducting significantly longer integrations (e.g., $\geqslant 1$ Gyr) in a reasonable amount of time.

We find that 5% of the 1σ test particles, 3% of the 10σ test particles, and 10% of the 100σ test particles exceed a heliocentric distance of 50 AU, and are effectively ejected from the asteroid belt, within 100 Myr (Figure 4). P/2006 VW$_{139}$ itself is found to be stable over the 100 Myr test period (neglecting non-gravitational forces), consistent with its Lyapunov time of $T_{lyap} > 1$ Myr, where a body is considered stable if $T_{lyap} > 100$ kyr (Tsiganis et al. 2003). No systematic distribution is evident for ejected 1σ or 10σ test particles, though 44% of 100σ test particles with $a < 3.04$ AU are ejected, perhaps due to the 9J:4A mean-motion resonance with Jupiter at 3.029 AU (Figure 4(b)). For reference, P/2006 VW$_{139}$ fluctuates between $a = 3.047$ AU and $a = 3.069$ AU over the course of our simulations.

As two MBCs (133P and 176P) belong to the $\sim$2.5 Gyr old (Nesvorný et al. 2003) Themis asteroid family, and 133P additionally belongs to the young < 10 Myr Beagle sub-family (Nesvorný et al. 2008), we perform a search for any family associations that P/2006 VW$_{139}$ may have. Employing hierarchical clustering method (Zappalà et al. 1990) analysis and analytically determined proper orbital elements retrieved on 2011 December 1 from AstDyS (http://hamilton.dm.unipi.it/astdys/), we compute the number of asteroids dynamically linked to P/2006 VW$_{139}$ as function of cutoff distance, d_c (in velocity space). At $d_c = 63$ m s^{-1}, we find a statistically significant clustering of 24 asteroids, which then merges with the Themis family at $d_c = 70$ m s^{-1} (Figure 4(c)). This possible P/2006 VW$_{139}$ sub-family is separated from the main Themis family by several two- and three-body mean-motion resonances (11J:5A, 3J-2S-1A, and 1J+3S-1A) with Jupiter and Saturn, though our dynamical simulations indicate these resonances may be only weakly destabilizing (Figure 4(b)). P/2006 VW$_{139}$'s association with the Themis family is interesting because of the family's aforementioned association with 133P, 176P, and possibly 238P (Haghighipour 2009), though more detailed study is needed to clarify the nature of this association, as well as the significance of the possible sub-family.

4. DISCUSSION

While spectroscopy did not reveal any evidence of gas emission (Section 3.3), morphological and photometric analyses (Section 3.2) strongly suggest that the activity of P/2006 VW$_{139}$ is cometary in nature, and not impact-driven. We conclude that this object is likely an MBC, making it the sixth such object discovered to date. The discovery circumstances of the known MBCs suggest that many more must exist, particularly in the outer main belt (Hsieh 2009). Therefore, we expect that current and next-generation all-sky surveys like Pan-STARRS
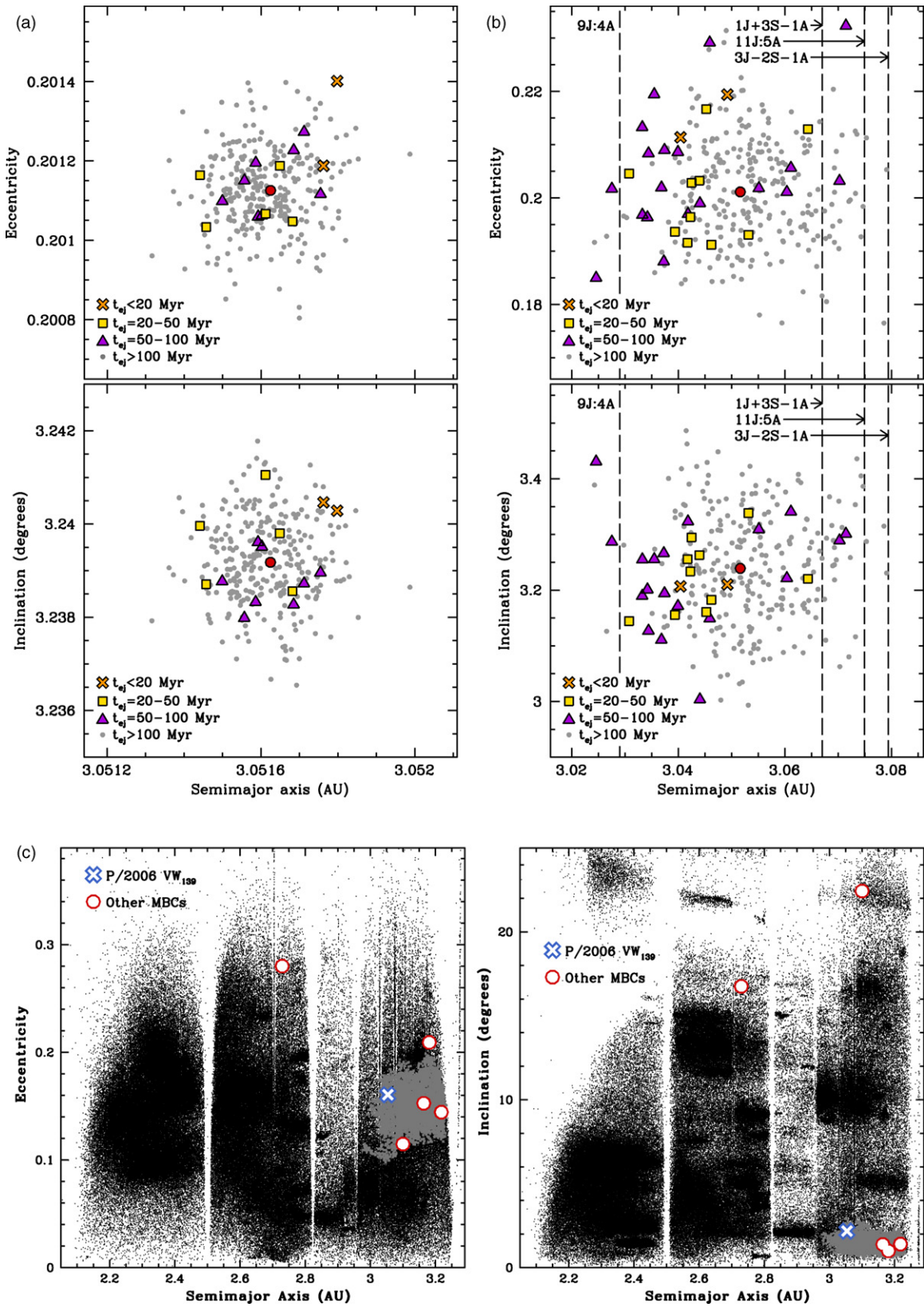
Figure 4. (a) Plots of semimajor axis versus eccentricity (top) and inclination (bottom) showing initial osculating elements of three 1σ sets of Gaussian-distributed test particles whose orbits are integrated for 100 Myr (Section 3.4), with the current osculating orbital elements of P/2006 VW$_{139}$ shown as a red circle at the center of each panel. Particles ejected in <20 Myr, between 20 Myr and 50 Myr, and between 50 Myr and 100 Myr are plotted with orange X symbols, yellow squares, and purple triangles, respectively, while particles that are not ejected within 100 Myr are marked with gray dots. (b) Same as (a) but for 100σ test particle sets, where the positions of the 9J:4A, 1J+3S-1A, 11J:5A, and 3J-2S-1A mean-motion resonances are marked with dotted lines. (c) Plots of proper semimajor axis vs. proper eccentricity (left) and proper inclination (right) of main-belt asteroids (small black dots), Themis family members (small gray dots), P/2006 VW$_{139}$ (blue X symbol), and other MBCs (red circles).

(A color version of this figure is available in the online journal.)

will reveal more of the true extent of the population in the coming years, provided that techniques can be deployed to efficiently screen for such objects amid the enormous amounts of data produced by these surveys. Thorough physical and dynamical investigations of each new discovered object will then be essential for first determining the most likely cause of the observed activity (cf. Hsieh et al. 2012a; Jewitt 2012), and then ascertaining the global properties of the population of objects confirmed as MBCs to better understand their implications for understanding terrestrial water delivery.

Additional observations of P/2006 VW$_{139}$ itself are encouraged until the end (in 2012 March) of the 2011–2012 observing window to monitor the decline of activity for comparison to other MBCs (cf. Hsieh et al. 2011c, 2012b). Observations during the 2012–2013 observing window, when the object may be largely inactive, should be useful for determining its nucleus properties. By adding to our knowledge of the properties of inactive MBC nuclei (cf. Hsieh et al. 2009a; Licandro et al. 2011), the latter observations will help us better understand the relationship of active MBCs to the inactive main-belt population, perhaps facilitating the development of more powerful search methods, such as targeted monitoring of extremely likely MBC candidates. Furthermore, robust protocols for identifying icy objects, even in the absence of activity (which is transient even for known MBCs), will be crucial for ascertaining the true abundance and distribution of ice in the asteroid belt.

REFERENCES

Aihara, H., Allende Prieto, C., An, D., et al. 2011, ApJS, 193, 29
Benn, C., Dee, K., & Agócs, T. 2008, Proc. SPIE, 7014, 229
Bodewits, D., Kelley, M. S., Li, J.-Y., et al. 2011, ApJ, 733, L3
Buzzoni, B., Delabre, B., Dekker, H., et al. 1984, ESO Messenger, 38, 9
Chambers, J. E. 1999, MNRAS, 304, 793
Elst, E. W., Pizarro, O., Pollas, C., et al. 1996, IAU Circ., 6456, 1
Finson, M. L., & Probstein, R. F. 1968, ApJ, 154, 327
Garradd, G. J., Sostero, G., Camilleri, P., et al. 2008, IAU Circ., 8969, 1
Gilbert, A. M., & Wiegert, P. A. 2009, Icarus, 201, 714
Haghighipour, N. 2009, Meteorit. Planet. Sci., 44, 1863
Hainaut, O. R., Kleyna, J., Sarid, G., et al. 2012, A&A, 537, A69
Haser, L. 1957, Bull. Soc. R. Sci. Liege, 43, 740
Hook, I. M., Jørgensen, I., Allington-Smith, J. R., et al. 2004, PASP, 116, 425
Hsieh, H. H. 2009, A&A, 505, 1297
Hsieh, H. H., Denneau, L., Wainscoat, R. J., et al. 2011a, CBET, 2920, 1
Hsieh, H. H., Ishiguro, M., Lacerda, P., & Jewitt, D. 2011b, AJ, 142, 29
Hsieh, H. H., & Jewitt, D. 2006, Science, 312, 561
Hsieh, H. H., Jewitt, D., & Fernández, Y. R. 2009a, ApJ, 694, L111
Hsieh, H. H., Jewitt, D. C., & Fernández, Y. R. 2004, AJ, 127, 2997
Hsieh, H. H., Jewitt, D., & Ishiguro, M. 2009b, AJ, 137, 157
Hsieh, H. H., Jewitt, D., Lacerda, P., Lowry, S. C., & Snodgrass, C. 2010, MNRAS, 403, 363
Hsieh, H. H., Meech, K. J., & Pittichová, J. 2011c, ApJ, 736, L18
Hsieh, H. H., Yang, B., & Haghighipour, N. 2012a, ApJ, 744, 9
Hsieh, H. H., et al. 2012b, AJ, in press
Ishiguro, M., Hanayama, H., Hasegawa, S., et al. 2011, ApJ, 741, L24
Jewitt, D. 2012, AJ, 143, 66
Jewitt, D., & Guilbert-Lepoutre, A. 2012, AJ, 143, 21
Jewitt, D., Weaver, H., Agarwal, J., Mutchler, M., & Drahus, M. 2010, Nature, 467, 817
Jewitt, D., Weaver, H., Mutchler, M., Larson, S., & Agarwal, J. 2011, ApJ, 733, L4
Jewitt, D., Yang, B., & Haghighipour, N. 2009, AJ, 137, 4313
Kinoshita, D., Chen, C.-W., Lin, H.-C., et al. 2005, Chin. J. Astron. Astrophys., 5, 315
Kolokolova, L., Hanner, M. S., Levasseur-Regourd, A.-C., & Gustafson, B. Å. S. 2004, in Comets II, ed. M. C. Festou, H. U. Keller, & H. A. Weaver (Tucson, AZ: Univ. Arizona Press), 577
Landolt, A. U. 1992, AJ, 104, 340
Licandro, J., Campins, H., Tozzi, G. P., et al. 2011, A&A, 532, A65
Lisse, C. M., A'Hearn, M. F., Hauser, M. G., et al. 1998, ApJ, 496, 971
Magnier, E. 2006, in Proc. Advanced Maui Optical and Space Surveillance Technologies Conference, ed. S. Ryan (Kihei: The Maui Economic Development Board), E50
Morbidelli, A., Chambers, J., Lunine, J. I., et al. 2000, Meteorit. Planet. Sci., 35, 1309
Nesvorný, D., Bottke, W. F., Levison, H. F., & Dones, L. 2003, ApJ, 591, 486
Nesvorný, D., Bottke, W. F., Vokrouhlický, D., et al. 2008, ApJ, 679, L143
Nomen, J., Marsden, B. G., Birtwhistle, P., et al. 2010, IAU Circ., 9169, 1
Reach, W. T., Sykes, M. V., Lien, D., & Davies, J. K. 2000, Icarus, 148, 80
Read, M. T., Bressi, T. H., Gehrels, T., Scotti, J. V., & Christensen, E. J. 2005, IAU Circ., 8624, 1
Schleicher, D. G. 2010, AJ, 140, 973
Snodgrass, C., Tubiana, C., Vincent, J.-B., et al. 2010, Nature, 467, 814
Sonnett, S., Kleyna, J., Jedicke, R., & Masiero, J. 2011, Icarus, 215, 534
Spahr, T. B., Williams, G. V., Marsden, B. G., Nakano, S., & Doppler, A. 2009, Minor Planets and Comets Orbit Supplement 157469, http://www.minorplanetcenter.net/iau/ECS/MPCArchive/2009/MPO_20090509.pdf
Tonry, J. L., et al. 2012, ApJ, submitted
Tsiganis, K., Varvoglis, H., & Morbidelli, A. 2003, Icarus, 166, 131
Yang, B., & Hsieh, H. H. 2011, ApJ, 737, L39
Zappalà, V., Cellino, A., Farinella, P., & Knežević, Z. 1990, AJ, 100, 2030